SCIENTIFIC REPORTS

OPEN

Residence time of singlet oxygen in membranes

V. S. Sokolov[1], O. V. Batishchev[1,2], S. A. Akimov[1,3], T. R. Galimzyanov[1,3], A. N. Konstantinova[1], E. Malingriaux[1], Y. G. Gorbunova[1,4], D. G. Knyazev[5] & P. Pohl[5]

Received: 18 December 2017
Accepted: 24 August 2018
Published online: 18 September 2018

Photodynamic therapy uses photosensitizers (PS) to kill cancer cells by generating reactive oxygen species – like singlet oxygen (SO) - upon illumination with visible light. PS membrane anchoring augments local SO concentration, which in turn increases photodynamic efficiency. The latter may suffer from SO's escape into the aqueous solution or premature quenching. Here we determined the time constants of SO escape and quenching by target molecules to be in the nanosecond range, the former being threefold longer. We confined PS and dipolar target molecules either to different membrane monolayers or to the same leaflet and assessed their abundance by fluorescence correlation spectroscopy or membrane surface potential measurements. The rate at which the contribution of the dipolar target molecules to membrane dipole potential vanished, served as a measure of the photo-oxidation rate. The solution of the reaction–diffusion equations did not indicate diffusional rate limitations. Nevertheless, reducing the PS-target distance increased photodynamic efficiency by preventing other SO susceptible moieties from protecting the target. Importantly, our analytical model revealed a fourfold difference between SO generation rates per molecule of the two used PSs. Such analysis of PS quantum yield in a membrane environment may help in designing better PSs.

Photosensitizers (PS) play a key role in cancer photodynamic therapy[1–3]. They adhere to cancer cells and kill them when excited by light due to the generation of reactive oxygen species (ROS)[4]. PS that respond to visible light may be tuned to mainly produce singlet oxygen (SO), which, in turn, preferentially targets membrane proteins. The efficacy of this approach crucially depends on (i) PS' membrane affinity[5], (ii) the quantum yield of SO generation, (iii) SO lifetime, τ_l, and (iv) SO dwell time τ_{dw} in the membrane.

SO residence time τ_r may be determined by either τ_l or τ_{dw}. Taking into account $^1O_2$ decay[6], SO may travel $\delta = \sqrt{D\tau_l} \approx 120\,nm$ in first case assuming a diffusion constant of $D = 5 \times 10^{-5}\,cm^2\,s^{-1}$[7]. $\tau_l \approx 3\,\mu s$ has been reported for a liposomal environment[8]. Thus, once born within the membrane, the likelihood of SO hitting the desired target would appear to be rather high, even if the cell membrane is sparsely decorated by PS molecules. In the second case τ_r is limited by SO's escape into the aqueous environment. The oxygen water/membrane distribution coefficient is equal to $K_p \approx 4.4$[9]. Assuming the same K_p for SO suggests that SO may hit the membrane-water interface no more than 4.4 times before escaping into the cytoplasm or the extracellular solution. If we take membrane thickness $d = 4\,nm$ as the characteristic diffusion span between the hits, we find $\tau_{dw} = d^2/D = 3\,ns$. This estimate is close to $\tau_{dw} = 12\,ns$ as predicted by molecular dynamics simulations[10]. Accordingly, τ_{dw}, would be much smaller than τ_l, indicating that the actual distance between PS and target molecules determines photodynamic efficiency. If so, an increase in diffusion span due to PS burial into the hydrophobic membrane interior should augment τ_{dw} (and thus τ_r), which in turn, could increase photodynamic efficiency. A correlation between PS penetration depth and photo effects has indeed been observed[11], however, the molecular mechanism has not yet been identified.

To distinguish between the possible scenarios: $\tau_r \approx \tau_l$, or $\tau_r \approx \tau_{dw}$, we adsorbed PS and dipolar target (DT) molecules at different densities either to the same or to opposing leaflets of a lipid membrane and analyzed effective encounters between SO and DT in terms of the rate at which DT's contribution to membrane dipole potential vanished. We observed τ_l to be in the nanosecond range indicating that SO rarely escapes from the membrane and that augmenting photodynamic efficiency requires shortening of the DT to PS distances.

[1]A.N. Frumkin Institute of Physical Chemistry and Electrochemistry, Russian Academy of Sciences, Moscow, Russia. [2]Moscow Institute of Physics and Technology, Dolgoprudny, Russia. [3]National University of Science and Technology "MISiS", Moscow, Russia. [4]N.S. Kurnakov Institute of General and Inorganic Chemistry, Russian Academy of Sciences, Moscow, Russia. [5]Institute of Biophysics, Johannes Kepler University Linz, Linz, Austria. Correspondence and requests for materials should be addressed to P.P. (email: peter.pohl@jku.at)

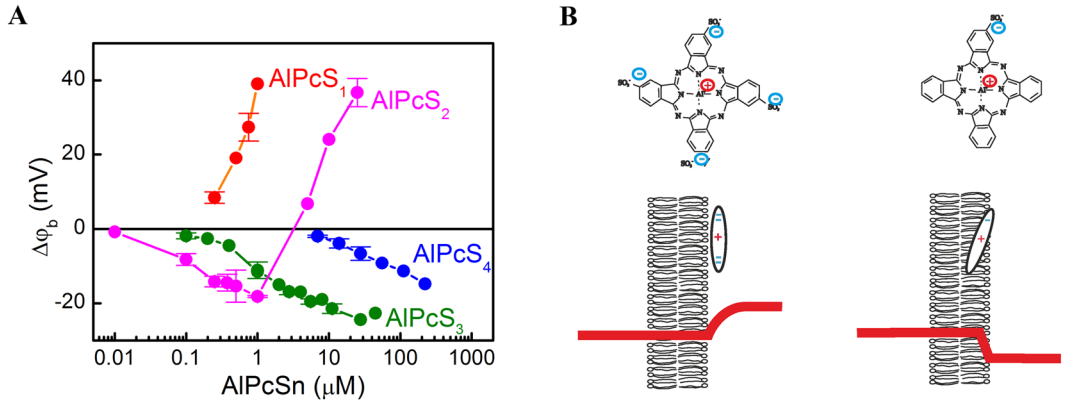

Figure 1. Adsorption of phthalocyanines on the bilayer lipid membrane. (**A**) Dependence of the boundary potential change $\Delta\varphi_b$ upon concentration of aluminum phthalocyanines with various numbers of sulfo groups in the solution. (**B**) The various positions of the phthalocyanines in the membrane with four and one sulfo groups resulting in the generation of the boundary potential of opposite signs on the surface of the lipid membrane. Red lines – the profiles of the potential change across the membrane due to adsorption of these phthalocyanines on the right side of the membrane.

Materials and Methods

Black lipid membranes (BLMs) were formed by the Mueller Rudin technique[12] from a solution containing 15 mg/ml L-α- diphytanoylphosphocholine (Avanti Polar Lipids, USA) per ml of n-decane in an aperture (diameter 0.8–1.2 mm) of a Teflon diaphragm that separated two aqueous compartments of equal volumes. Both compartments were continuously stirred by magnetic stirrers. Buffer solutions were prepared in twice distilled water with 100 mM KCl (chemically pure, Reachim, Russia) and 10 mM HEPES (Calbiochem, USA) at pH 7.5, adjusted by KOH (chemically pure, Reachim, Russia). The styryl dye 4-(2-(6-(Dibutylamino)-2-naphthalenyl) ethenyl)-1-(3-sulfopropyl)pyridinium hydroxide (di-4-ANEPPS; Sigma, USA) and aluminum phthalocyanines, AlPcSn, with various numbers n ($1 \leq n \leq 4$) of peripheral sulfo-groups from (Porphyrin Products, USA) served as DT and PS, respectively.

The electrical measurements were performed with the aid of silver-chloride electrodes that were connected to the aqueous compartments via agar bridges. Total electrode resistance did not exceed 30 kOhm. Membrane capacitance and conductance were continuously measured as previously described[13]. The difference of BLM boundary potentials, $\Delta\varphi_b$, was monitored by using the intramembrane field compensation (IFC) method[13,14] (see also reviews[15,16]). IFC uses a variable dc offset to a sine wave input (300–700 Hz) to minimize membrane capacitance. We measured $\Delta\varphi_b$ and determined the photo–oxidation rate of DT as previously described[17]. In brief, we placed the planar lipid bilayer into the focused beam of a monochromatic light source (semiconductor diode laser with a wavelength of 670 nm, optical power 1 mW). Subsequently, we added the PS into the distant aqueous compartment (also called *cis* compartment) with respect to the light source. DT was added either to the *cis* compartment or to the opposite (*trans*) compartment. Since both substances are membrane impermeable, their location remained well defined throughout the experiment".

The membrane surface densities, T and P, as well as the lateral diffusion coefficients, D_{DT} and D_{PS} of both DT and PS were assessed by placing the horizontal BLM formed by Montal-Mueller technique[18] into the focus of a laser scanning microscope (LSM 510 META/ConfoCor 3, Carl Zeiss, Jena, Germany) and exploiting fluorescence correlation spectroscopy, FCS[19,20]:

$$D_{DT,PS} = \frac{r^2}{4\tau_d}, \tag{1}$$

where r and τ_d are the lateral focus radius of the confocal volume and the characteristic residence time of DT or PS in the confocal volume, respectively. τ_d was obtained by fitting a one-component model for 2D translational diffusion[21] to the autocorrelation function G of the time, τ, dependent fluorescence intensity:

$$G(\tau) = 1 + \frac{1}{N(1 + \tau/\tau_D)}, \tag{2}$$

where N is the average number of fluorescent molecules in the confocal volume.

Results

PS adsorption to the lipid bilayer. PS membrane adsorption alters bilayer boundary potential φ_b. The introduced change $\Delta\varphi_b$ depends upon PS' aqueous concentration, P_a[5,13] (Fig. 1A). Generally, $\Delta\varphi_b$ is a superposition of changes in membrane surface potential $\Delta\varphi_s$ and membrane dipole potential $\Delta\varphi_d$[15,16]:

$$\Delta\varphi_b = \Delta\varphi_s + \Delta\varphi_d \tag{3}$$

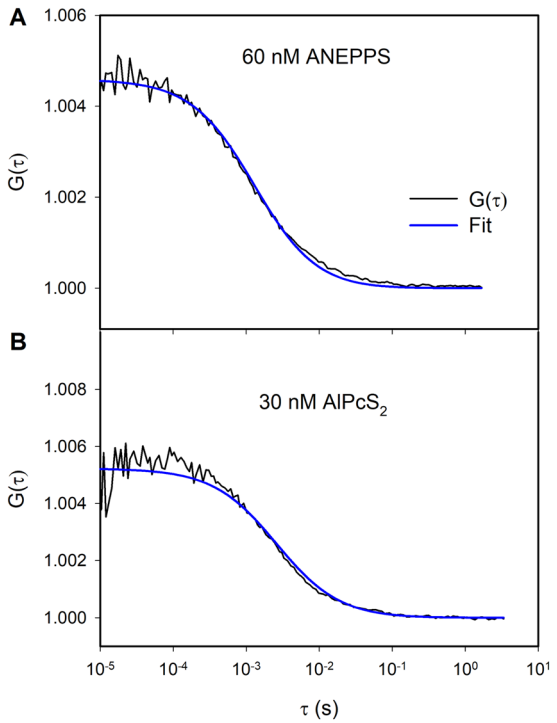

Figure 2. (**A**) Autocorrelation function of fluorescence of di-4-ANEPPS (concentration in solution is 60 nM) and its approximation by the equation (2). (**B**) Autocorrelation function of fluorescence of $AlPcS_2$ (concentration in solution is 30 nM) and its approximation by the equation (2). BLM formed by the Montal-Mueller technique by adding the solution of diphytanoylphosphatidylcholine in hexane (15 mg/ml) to the water-air interface.

φ_s is accessible via measurements of the electrophoretic mobility of lipid vesicles. The mobility reflects the so-called ζ – potential that, in 0.1 M KCl, describes the electrostatic potential at 0.2 nm distance from the vesicle surface. Using the Gouy Chapman theory, φ_s can be calculated from ζ. Upon $AlPcS_3$ and $AlPcS_4$ membrane adsorption, we measured $\Delta\varphi_b$ values that can entirely be attributed to changes in ζ[5], i.e. $\Delta\varphi_b$ and $\Delta\varphi_s$ are roughly identical.

In contrast, for $AlPcS_1$ and $AlPcS_2$ negative ζ – values[5] (and thus negative $\Delta\varphi_s$ values) have been observed for all aqueous PS concentrations P_a, while $\Delta\varphi_b$ was positive for some $AlPcS_2$ concentrations and all $AlPcS_1$ concentrations. The observation suggests that both $AlPcS_2$ and $AlPcS_1$ significantly alter $\Delta\varphi_d$. The underlying dipole moment of the phthalocyanine molecule is generated by the separation of the positive charge at the aluminum cation in the center and the negative charges of the sulfo-groups on its periphery. Thus, in contrast to $AlPcS_4$, the charges in $AlPcS_1$ are distributed asymmetrically (Fig. 1B). The positive sign of $\Delta\varphi_d$ indicates that $AlPcS_1$ inserts the positive Al-moiety into the lipid bilayer, whereas the negatively charged S-group faces the aqueous solution (Fig. 1B). $AlPcS_2$ is likely to adopt a similar orientation (Fig. 1B). Our result is in line with $AlPcS_n$ accessibility by fluorides[5] and molecular dynamic simulations with porphyrin[22].

Determination of membrane surface PS and DT densities. We performed FCS experiments to find T and P (Fig. 2). DT elicits $\Delta\varphi_b$ changes that are proportional to its aqueous concentrations[17]. That is, DT's limited aqueous solubility prevents the linear relation between T_a and T from breaking down as might be expected in case of a Langmuir adsorption isotherm. Since $\Delta\varphi_b$ and the aqueous DT concentration T_a are the proportional to each other[17], there must be a linear relationship between T_a, and T. It allowed calculating that T amounts to 30 molecules per μm^2 and per nM of T_a. Thus, for $T_a = 60$ nM we find $T = 1800$ molecules μm^{-2} (Fig. 2A). Accordingly, DT's contribution to $\Delta\varphi_b$ amounts to 0.003 molecules/nm^2/mV.

From $\tau_{DT} = 1.31$ ms, we found $D_{DT} = 7.6\,\mu m^2/s$ (Eq. 2). We used FITC (fluorescein isothiocyanate) for calibration experiments. Its diffusion coefficient D_{FITC} is equal to $565\,\mu m^2/s$[23,24]. From the equation:

$$V = \pi^{\frac{3}{2}}(\omega_r^2)^{\frac{3}{2}}S = \pi^{\frac{3}{2}}(4D_{FITC}\tau_{FITC})^{\frac{3}{2}}S \quad (4)$$

we determined the confocal volume $V = 0.22$ fl. The structural parameter S (defined as the ratio of the long (ω_z) to the short radii ($\omega_x = \omega_y = \omega_r$) of the ellipsoidal confocal volume and τ_{FITC} were equal to 5 and 18 μs, respectively.

Similarly, we obtained $D_{PS} = 3.4\,\mu m^2/s$ from PS residence time in the focal plane $\tau_{PS} = 2.6$ ms. At an aqueous $AlPcS_2$ concentration $P_a = 30$ nM (Fig. 2B), we observed $P = 1700$ molecules/μm^2. The corresponding adsorption coefficient amounts to 57 molecules/μm^2 per nM P_a. The focal volume of the red laser was calibrated with Cy5.

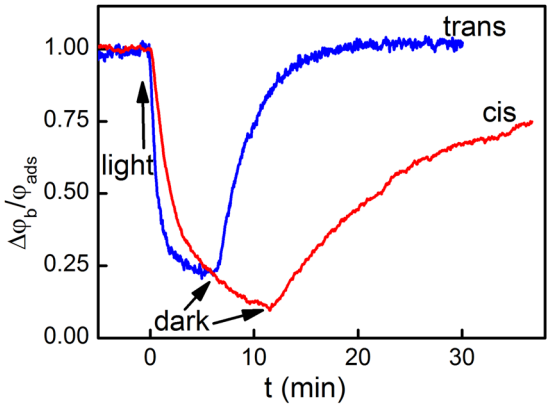

Figure 3. Comparison of the kinetics of relative potential decay during illumination and its recovery in the dark in case of cis and trans photo effects. Either the *cis* or the *trans* solutions contained 2 μM di-4-ANEPPS ("cis" photo effect or "trans" photo effect, respectively). 0.2 μM $AlPcS_2$ were added to the cis solution.

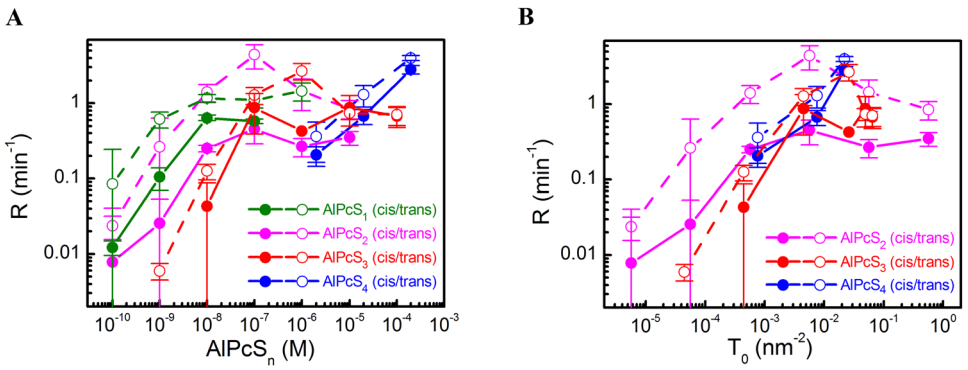

Figure 4. Dependence of the rate *R* of oxidation of di-4-ANEPPS adsorbed on the *cis* (open symbols) or *trans* (closed symbols) side of the BLM on the aqueous $AlPcS_n$ concentration (**A**) or as a function of $AlPcS_2$ and $AlPcS_4$ membrane surface densities (**B**).

We took Cy5's diffusion coefficient and *S* to be equal to 280 μm^2/s[25,26] and 8, respectively. Cy5's residence time τ_{Cy5} amounted to 31.6 μs.

The photodynamic activity of phthalocyanines with various numbers of sulfo-groups. When both DT and PS were adsorbed to the BLM surface, membrane illumination at 670 nm led to a drop in $\Delta\varphi_b$ due to DT's oxidation by SO[17]. $\Delta\varphi_b$ recovered in the dark due to the adsorption of intact DT molecules from the aqueous bulk solution (Fig. 3). The kinetics of photo damage depended on whether DT and PS were added into the solution to the same (*cis* configuration) side or to the opposite (*trans* configuration) side of the membrane. Dividing $\Delta\varphi_b(t)$ by its value φ_{ads} at time $t = 0$ we define the rate *R* of DT oxidation as[17]:

$$R = \frac{1}{\phi_{ads}} \frac{d\phi(t)}{dt}\bigg|_{t=0}, \tag{5}$$

enabling a quantitative analysis of the photodynamic effects. We found that *R* depended (i) on the number of sulfo-groups per PS molecule (Fig. 4A), (ii) the geometrical arrangement (*cis* or *trans* configuration), and (iii) the aqueous PS concentration. For PS molecules with two sulfo-groups, *R* depended non-monotonically on P_a in *trans* configuration. Similar bell-shaped concentration dependencies were reported for SO-mediated gramicidin inactivation[5]. In contrast, *R* increased monotonically with P_a in *cis* configuration, suggesting that SO quenching by PS may be involved. This would be in line with chemoluminescence-based observations of SO quenching by PS[27].

In order to account for differences in $AlPcS_n$ membrane affinities, we replotted *R* as a function of *P* (Fig. 4B). For $AlPcS_3$ and $AlPcS_4$, we calculated *P* from the increment in surface charge[5], whereas we used FCS to determine *P* of the weakly charged $AlPcS_2$ and $AlPcS_1$. *R* did not significantly vary with the number of sulfogroups in *cis* configuration: *R* was roughly proportional to *P* for $P < 0.01$ molecules/nm^2, and it approached saturation at higher *P*. However, in *trans* configuration, we observed a 10-fold augmented *R* for $AlPcS_2$ and the absence of saturation for $AlPcS_4$. The latter may be due to $AlPcS_4$'s low binding constant.

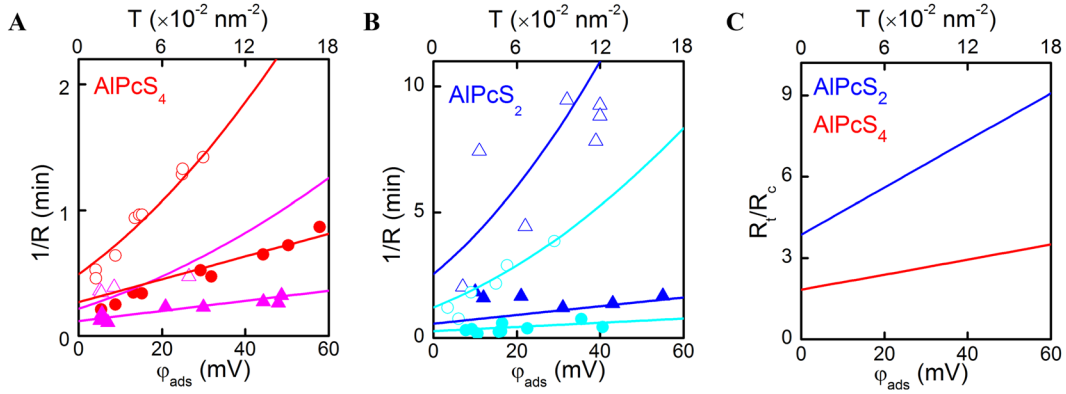

Figure 5. Dependence of the inverse rate of cis and trans photo effects on the potential caused by adsorption of di-4-ANEPPS at (**A**) 20 μM (squares) or 200 μM of $AlPcS_4$ (down triangles) and (**B**) 4 nM (up triangles) or 200 nM (circles) of $AlPcS_2$ in water solution. The filled symbols represent the experiments where di-4-ANEPPS was at *trans* side of the BLM, the open ones – at the *cis* side. The spline lines are best fits of the theoretical model (equations T4 and T5) to the data. (**C**) $R_t/R_c = f(T_0)$ plot from the results of the fit.

Mathematical model. Our counterintuitive observation that R is smaller if PS and DT are adsorbed to the same leaflet than to opposite ones has three possible explanations: (1) PS and DT molecules interact with each other thereby decreasing the quantum yield of SO, (2) PS molecules quench SO or (3) DT molecules possess two different moieties that may serve as a SO target: damage of only one of these moieties - of the aniline group - changes membrane dipole potential, whereas targeting the second moiety - the unsaturated hydrocarbon chain in the middle of the molecule - remains electrically silent.

First, we ruled out the potential interaction by recording the effect of DT on the fluorescence spectra of liposomal PS (see Supplementary Fig. S1). Since there was none, a DT-PS interaction is unlikely. Second, we estimated the impact of PS mediated SO quenching. Since it should depend on the concentration of both molecules, we would expect the ratio R_c/R_t to vary with PS concentration. The invariance of that ratio at low PS concentrations (Fig. 4) excludes SO quenching by PS from being responsible for the difference between R_c and R_t. Third, to estimate the impact of SO quenching by DT molecules, we plotted 1/R against φ_{ads} (Fig. 5). The slopes of the curves in "*cis*" configuration exceeded the slopes in "*trans*" configuration for all φ_{ads}, thereby confirming DT's quenching effect. The difference between the two configurations was more pronounced when $AlPcS_4$ was substituted for $AlPcS_2$, suggesting a deeper bilayer penetration depth of $AlPcS_2$, and thus, a smaller PS to DT distance.

Differences in the oxidation rates of styryl dyes analogues[17] indicate that DT possess two different moieties that may serve as a SO target: damage of only one of these moieties - of the aniline group - changes membrane dipole potential, whereas targeting the second moiety - the unsaturated hydrocarbon chain in the middle of the molecule - remains electrically silent. This peculiarity generates the different *R* in *cis* and *trans* configurations: In *cis* configuration, DT's naphthalene ring is only ~ 1 nm farther away from the PS molecule than DT's double bond (Fig. 6). Consequently, the double bond may provide protection for the naphthalene ring. In *trans* configuration, the naphthalene ring is closer to the PS molecule, and thus, it may represent the primary SO target. This hypothesis only makes sense if τ_r is very short – small enough to prevent SO from reaching distant targets, and definitely much shorter than suggested by the previously estimated $\tau_l = 3$ μs in a liposomal suspension.

We supported the hypothesis about 2 SO susceptible DT moieties with a mathematical model that takes into account all chemical reactions and membrane diffusion processes (see Theory). The numerical solution of the differential equations satisfactorily fits the experimental data (Fig. 5) for the parameter set displayed in Table 1. The model divides the lipid membrane into three layers and assumes that SO is generated by PS molecules in one of the outer layers. In contrast, DT molecules extend from the outer to the middle layer. The $\Delta\varphi_d$ affecting moiety (designated by letter T in Fig. 6) - the naphthalene group at the end of the chromophore molecule - is immersed into the middle layer[17]. The other moiety that is susceptible to SO – the unsaturated hydrocarbon chain in the middle of the molecule (designated by letter S in the Fig. 6) – localizes to one of the outer membrane layers. SO may quench the S-group even when the T-moiety is oxidized and DT's contribution to $\Delta\varphi_d$ has vanished.

We noticed that - contrary to the expectations - the limit of the oxidation rate at zero DT density depends on which side of the membrane contains DT (Fig. 5). This observation suggests that the DT preparation already contained oxidized molecules, which were capable of capturing SO, while being unable to contribute to $\Delta\varphi_b$.

Theory

Mathematical model of SO generation, membrane permeation, and quenching. The model describes the permeation of singlet oxygen through the membrane taking into account the non-uniform distribution of SO across the membrane. SO mirrors the bell–shaped distribution of ground-state oxygen with the concentration maximum in the middle of the membrane[10]. The steady-state concentration of SO not only depends on this distribution, but also on its lifetime. To simplify this distribution, we will consider it to be discrete. Let the membrane consist of three layers, two of them are the fields of the lipid bilayer lying near its interface with water, and the third one – the internal hydrophobic region of the membrane, is located in the layers of hydrocarbon

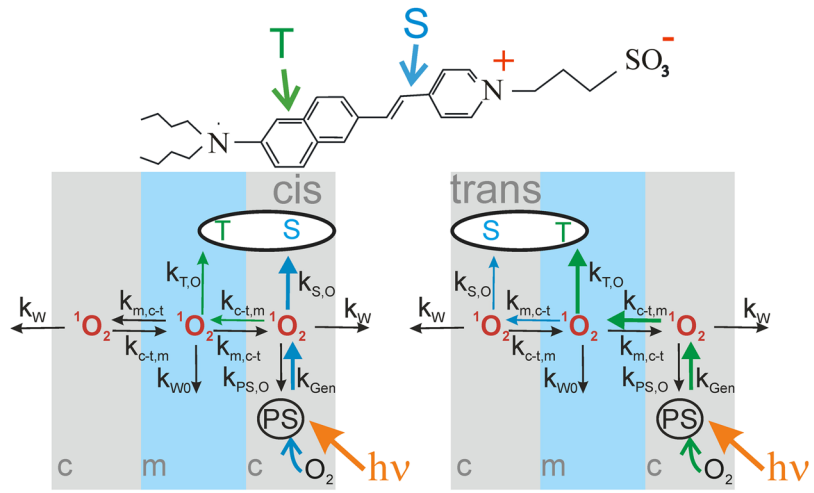

Figure 6. Model of SO generation, quenching and transport. (**A**) ANEPPS' structure reveals two different moieties that can be targeted by SO: the aniline ring (T) and the unsaturated hydrocarbon chain (S). (**B**) SO generation, membrane transport, and quenching. After oxidation of the aniline ring, the target molecule loses its dipole moment (or its orientation), but the hydrocarbon double bond may still quench SO.

Phthalocyanine	$AlPcS_4$	$AlPcS_2$
k_{Gen} $(m^2 s^{-1})$	0.6 ± 0.1	2.4 ± 0.3
$\boldsymbol{k_W}$ $\boldsymbol{(s^{-1})}$	$(5.0 \pm 0.9) \cdot 10^7$	
$\boldsymbol{k_{W0}}$ $\boldsymbol{(s^{-1})}$	$(2.9 \pm 0.3) \cdot 10^7$	
$\boldsymbol{k_{T,O}}$ $\boldsymbol{(m^2 s^{-1})}$	$\boldsymbol{>10^{-10}}$	
$k_{S,O}$ $(m^2 s^{-1})$	$(1.5 \pm 0.2) \cdot 10^{-10}$	$(6.0 \pm 0.7) \cdot 10^{-10}$
$k_{c-t,m}$ $(s^{-1})^{fixed,\ from\ Pm}$	$2.4 \cdot 10^8$	
$k_{m,c-t}$ $(s^{-1})^{fixed,\ from\ Pm}$	$5.5 \cdot 10^7$	

Table 1. Model parameters. They represent the best fit of the system of differential equations (T4) to the experimental data (Fig. 5A,B). The global parameters (independent on the choice of the phtalocyanine) are highlighted in bold. The local parameters, i.e. the rate, k_{Gen}, of SO generation and the rate, $k_{S,O}$, of SO quenching by S, are valid for all concentrations of the specific phtalocyanine.

chains of the lipids. We will refer to these layers as *cis* (the layer with the PS molecules), medium (the middle of the membrane) and *trans* (the layer opposite to cis). The concentrations of singlet oxygen in these layers will be designated as O_c, O_m and O_t, correspondingly. The singlet oxygen is generated from the excited molecules of PS adsorbed on the cis-side of membrane. No matter which of the locations of the PS molecules is considered, ground state oxygen is present at saturating concentrations with respect to SO generation. Consequently, both $AlPcS_2$ and $AlPcS_4$ operate at a rate that is solely governed by light intensity (see for example Fig. 5 in[13] or Fig. 8 in[17]).

The target of SO can be located either in the cis or trans layer. The model assumes that two parts of the target molecule react with singlet oxygen (Fig. 6). The first one, the aniline group is designated by "T". The oxidation of this group by singlet oxygen in the middle layer (O_m in Fig. 6) nullifies their contribution to membrane dipole potential. The concentrations of this group in cis and trans layers are correspondingly designated, as T_c and T_t. The other part – the unsaturated hydrocarbon chain in the middle of the molecule (designated by "S" in Fig. 6) can react with singlet oxygen in the surface layers (O_c, or O_t) without changing the dipole potential. The approach neglects the incremental diffusion span of no more than 0.5 nm that a SO molecule has to cross if born on the "wrong" (opposite to the direction of movement) side of a PS molecule. It corresponds to travel time of only ~ 1 ns, which is at least 10 times smaller than the most conservative estimate of $\tau_{dw} = 12$ ns from molecular dynamics simulations[10].

The reactions and transfer of singlet oxygen in *cis* and *trans* photoeffects are shown in Fig. 6. The singlet oxygen can react with target molecules, be quenched by the medium, the molecules or photosensitizer and transfer to the adjacent layer. Once SO has left the membrane, the probability of its retrieval is negligible since (i) the volume of the aqueous bulk so much larger than that of the membrane, (ii) and the lifetime in aqueous solutions is very limited. The equations describe the damage of the target and the processes with singlet oxygen in the experiment, where the target molecules located at the *cis* side of the membrane are

$$\begin{cases} \dfrac{dT_c(t)}{dt} = k_{Sol,Mem}T_S - k_{Mem,Sol}T_c(t) - k_{T,O}T_c(t)O_m(t), \\ \dfrac{dO_c(t)}{dt} = k_{Gen}PS - k_{S,O}S_c(t)O_c(t) - (k_{PS,O}PS + k_{c-t,m} + k_W)O_c(t) + k_{m,c-t}O_m(t), \\ \dfrac{dO_m(t)}{dt} = k_{c-t,m}(O_c(t) + O_t(t)) - (2k_{m,c-t} + k_{W0})O_m(t) - k_{T,O}T_c(t)O_m(t), \\ \dfrac{dO_t(t)}{dt} = k_{m,c-t}O_m(t) - (k_{c-t,m} + k_W)O_t(t), \end{cases} \quad \text{(T1)}$$

where

k_a — rate constant of adsorption of target molecules from solution to membrane;
k_d — rate constant of desorption of target molecules from membrane to the solution;
$k_{T,O}$ — rate constant of damaging of target molecules by singlet oxygen;
k_{Gen} — rate constant of generation of singlet oxygen;
$k_{S,O}$ — rate constant of quenching of singlet oxygen by the target molecules;
$k_{PS,O}$ — rate constant of quenching of singlet oxygen by the photosensitizer molecules;
$k_{c\text{-}t,m}$ — rate constant of transfer of singlet oxygen from cis or trans layers to the middle one;
$k_{m,c\text{-}t}$ — rate constant of transfer of singlet oxygen from the middle layer to cis or trans ones;
k_W — rate constant of quenching of singlet oxygen in cis and trans layers;
k_{W0} — rate constant of quenching of singlet oxygen in the middle layer.

Similarly, the equations describing the damage of the target at the *trans* side are

$$\begin{cases} \dfrac{dT_t(t)}{dt} = k_{Sol,Mem}T_S - k_{Mem,Sol}T_t(t) - k_{T,O}T_t(t)O_m(t), \\ \dfrac{dO_c(t)}{dt} = k_{Gen}PS - (k_{PS,O}PS + k_{c-t,m} + k_W)O_c(t) + k_{m,c-t}O_m(t), \\ \dfrac{dO_m(t)}{dt} = k_{c-t,m}(O_c(t) + O_t(t)) - (2k_{m,c-t} + k_{W0})O_m(t) - k_{T,O}T_t(t)O_m(t), \\ \dfrac{dO_t(t)}{dt} = -k_{S,O}S_t(t)O_t(t) + k_{m,c-t}O_m(t) - (k_{c-t,m} + k_W)O_t(t). \end{cases} \quad \text{(T2)}$$

To simplify the solution of these equations, we will consider that the processes described here are fast when compared with the processes of oxidation and diffusion of the targets described in[17]. If the concentration of the singlet oxygen changes much faster than that of the targets, it reaches the steady-state value before the concentration of the target significantly begins to change. Therefore, we can solve the equations assuming the steady-state distribution of singlet oxygen and equilibrium distribution of the targets.

$$\frac{dO_c(t)}{dt} = \frac{dO_m(t)}{dt} = \frac{dO_t(t)}{dt} = 0 \quad \text{(T3)}$$

In this case, the equations for the singlet oxygen concentration transform to the algebraic ones. By solving these equations and introducing the steady-state concentrations of the singlet oxygen into the first equations in (T1) and (T2) we only have single differential equations describing the kinetics of oxidation of the target either in cis or in trans positions. Thus we will instead solve these equations by determining the rate of oxidation of the target R_c and R_t at cis and trans positions, respectively, as a slope (time derivative) of the relative change of the potential at the beginning of illumination according to Eq. 5. The relation between the potential measured in the experiment and the surface density of the target molecules can be established experimentally by comparing the dipole potentials measured by IFC method at given concentration of the ANEPPS in the solution (the data in[17]) and the surface density of these molecules measured by the FCS technique (Fig. 2). These values are proportional to each other:

$$\varphi = \alpha T_c, \text{ or } \varphi = \alpha T_t, \quad \text{where } \alpha = 4.65 \cdot 10^{-19}\text{V} \cdot \text{m}^2.$$

Relative potential can be derived through the ratio of current surface density of the target to the initial one corresponding to equilibrium of targets between the membrane and solution before the illumination

$$\varphi_{\text{Rel}}(t) = \frac{\varphi(t)}{\varphi_{ads}} = \frac{T_c(t)}{T_0} = \frac{T_t(t)}{T_0},$$

where

$$T_0 = T_{c0} = T_{t0} = T_s\frac{k_{Sol,Mem}}{k_{Mem,Sol}}.$$

In these designations, the R_c can be derived through the steady-state concentrations of singlet oxygen O_m determined by equations (T1)

$$R_c = -\left.\frac{d\phi_{Rel}(t)}{dt}\right|_{t=0} = -\frac{1}{T_0}\left.\frac{dT_c(t)}{dt}\right|_{t=0} = k_{T,O}O_m,$$

and similarly R_t – through O_m determined by equations (T2)

$$R_t = -\left.\frac{d\phi_{Rel}(t)}{dt}\right|_{t=0} = -\frac{1}{T_0}\left.\frac{dT_t(t)}{dt}\right|_{t=0} = k_{T,O}O_m$$

For further simplification of equations (T1 and T2), we will neglect SO quenching by PS, putting the corresponding constant, $k_{PS,O}$, equal to 0. It may be valid if we use very low concentrations of photosensitizers in the linear region of the dependence of the rate R on the concentrations of photosensitizers in the solution or on their surface densities (Fig. 4). It seems natural to assume that the surface densities of two parts of the same targets molecule, T and S, are equal. However, one cannot exclude the existence of a fraction of the target molecules, which are partially damaged and do not contribute to the dipole potential, but still can react with singlet oxygen and quench it. To take into account these "invisible" target molecules we will assume that surface density at each side of the membrane consists of two members: "visible" T and "invisible" S_0

$$S_c = T_c + S_0,\ \ S_t = T_t + S_0$$

Solving the equations (T1 and T2) with the above-mentioned simplifications gives the rates R_c and R_t as functions of the ANEPPS adsorption potential

$$\begin{aligned}\frac{1}{R_c} &= a_1\phi^2 + a_2\phi + a_3\\ \frac{1}{R_t} &= \frac{1}{R_c}\frac{b_1}{b_2 + \alpha S_0}\end{aligned} \tag{T4}$$

with

$$a_1 = \frac{k_{S,O}}{k_{c-t,m}\cdot k_{Gen}\cdot PS\cdot \alpha^2},\ s\cdot V^{-2}$$

$$b_1 = \alpha\frac{k_{c-t,m}+k_W}{k_{S,O}},\ V$$

$$b_2 = b_1 + \varphi_0,\ V$$

$$a_2 = \frac{k_{S,O}}{k_{c-t,m}\cdot k_{Gen}\cdot PS\cdot \alpha\cdot k_{T,O}}\left(\frac{2\varphi_0 k_{T,O}}{\alpha} + \frac{k_{T,O}(k_{c-t,m}+k_W)}{k_{S,O}} + k_{W0} + k_{m,c-t} + \frac{k_{m,c-t}\cdot k_W}{k_{c-t,m}+k_W}\right),\ s\cdot V^{-1}$$

$$a_3 = a_2\varphi_0 - a_1\varphi_0^2 + \frac{2k_{m,c-t}k_W + (k_{c-t,m}+k_W)k_{W0}}{k_{c-t,m}k_{Gen}\cdot PS\cdot k_{T,O}},\ s$$

We used equation T4 to fit the data in Fig. 5. $k_{c\text{-}t,m}$ was not used as a fitting parameter. but was obtained from the known membrane permeability $P_M = 80$ cm/s of O_2[28,29] that we assume to be equal to P_M of SO: $P_M = K_p\frac{D_M}{\delta}$, where δ is the membrane thickness. Substituting SO's membrane diffusion coefficient D_M by the Einstein relation, we find $P_M = K_p\frac{\delta^2}{2\tau\delta} = K_p\frac{\delta}{2\tau}$. Since we are not interested in the time τ that SO takes to cross the bilayer, but in the time that SO requires to diffuse from the middle of one of the outer layers to the middle of the membrane, we substitute δ and $1/\tau$ for $\delta/3$ and $k_{c\text{-}t,m}$, respectively. This yields $k_{c-t,m} = 2.4\times10^8\ s^{-1}$.

S_0 was treated as a constant parameter for each of PS and was found from the global fit as $\alpha S_0 = 30$ mV, equal both for $AlPcS_2$ and $AlPcS_4$.

One of the simplest consequences of the model is that the ratio of R_c and R_t is always less than 1. This ratio is equal to

$$\frac{R_c}{R_t} = \frac{b_1}{b_2 + \alpha S_0} = \frac{k_{c-t,m}+k_W}{k_{c-t,m}+k_W+k_{S,O}(T_0+S_0)} \tag{T5}$$

Discussion

Our experiments revealed that SO in membranes is extremely short-lived: instead of spending microseconds in the membrane interior, SO does not survive tens of nanoseconds. In other words, $\tau_r \approx \tau_l$. τ_l is mainly governed by the time it takes SO to reach its nearest target. The conclusion is based on experiments, in which a SO molecule that was born in the membrane headgroup region was free to target molecules in (i) the same headgroup region, (ii) the inner hydrophobic layer, and (iii) the opposing headgroup region. Although the increment in distance between these targets was smaller than 2 nm, the probability of SO reacting with the targets sharply decreased with distance.

A lower limit of τ_l maybe obtained by assuming a diffusion limited reaction. In our experiments, the DT molecules (for $\varphi_{ads} = 20$ mV) were only 4 nm apart as indicated by FCS measurements. Thus, in *cis* configuration, the distance r between a PS and the nearest DT neighbor molecule did not exceed 2 nm. Taking into account SO's diffusion coefficient $D = 5 \times 10^{-5}$ cm^2 s^{-1} [7], we find the SO travel time

$$\tau_t = \frac{r^2}{D} = 0.8\ ns \tag{6}$$

τ_t is probably smaller in biological membranes since they are densely packed with SO scavengers that are represented by unsaturated lipids and membrane proteins containing aromatic residues[30–33].

In order to obtain a more accurate estimate of τ_l, we performed a quantitative analysis of our experiments by solving the differential equations for the combined system of chemical reactions and diffusion processes (see Theory). We found the simplified solution represented by Eq. (7):

$$\frac{R_t}{R_c} = 1 + \frac{k_{S,O}(T_0 + S_0)}{k_{c-t,m} + k_W} \tag{7}$$

where T_0, S_0, R_c, and R_t denote T prior to illumination, the initial surface density of DT's oxidizable moiety that does not contribute to $\Delta\varphi_b$ (Fig. 6), R in *cis* and *trans* configurations, respectively. The R_t/R_c ratio depends on the combined rate k_W of SO membrane exit and quenching by the aqueous medium, the transfer rate $k_{c\text{-}t,m}$ from the outer membrane layer to the medium layer, and the rate $k_{S,O}$ of SO quenching by the S moiety of DT (Fig. 6). Eq. 7 assumes a non-negligible value S_0, i.e. it does not work for $T_0 \gg S_0$. Equation (7) predicts that R_c is always smaller than R_t, which is in perfect agreement with the experiment.

We first globally fitted the complete set of differential equations (see Theory) to individual sets of $R_c = f(T_0)$ and $R_t = f(T_0)$ that have been experimentally obtained for both $AlPcS_4$ and $AlPcS_2$ (Table 1 and Fig. 5A,B) and then constructed the $R_t/R_c = f(T_0)$ plot from the results of the fit (Fig. 5C). Solving the complete set of equations also allowed us to obtain the rate k_{Gen} of SO generation. k_{Gen} is fourfold higher for $AlPcS_2$ than for $AlPcS_4$, indicating either an environmental effect on SO yield or immediate SO escape into the aqueous solution without ever entering the lipid membrane. Indeed, in contrast to $AlPcS_4$'s four negative charges, which ensure that it lies flat on the membrane surface, $AlPcS_2$ penetrates into the bilayer. Its chromophore ring inclines towards the hydrocarbon core as indicated by a substantial contribution of $\Delta\varphi_d$ to $\Delta\varphi_b$. Thus, $AlPcS_2$'s ring is exposed to a four-fold higher oxygen concentration than that belonging to $AlPcS_4$. The observed increment in k_{Gen} agrees well with the previously reported increase of photosensitizer efficiency with increasing hydrophobicity[11,34,35].

Our mathematical model revealed the reaction rates of SO with targets: The rate $k_{T,O}$ of SO quenching by the T moiety of DT is roughly equal to $k_{S,O} \geq 6.0 \cdot 10^{-10}$ m^{2}s^{-1}. Taking into account the target density of about 0.1 molecule nm^{-2}, this value translates into a reaction time $\tau_{T,O} \approx 16$ ns of the T moiety with SO. $\tau_{T,O}$ is three orders of magnitude smaller than the estimate for τ_l from experiments[36] with non-oxidizable lipids, underpinning the conclusion that the main determinant of SO lifetime is target density. Moreover, τ_l is not diffusion limited, i.e. it is not governed by τ_t: $\tau_l \approx \tau_{T,O} \gg \tau_t$.

The mathematical model also allows assessing τ_{dw}. From $k_{m,c-t} = 5.5 \times 10^7$ s^{-1} and $k_w = (5.0 \pm 0.9) \times 10^7$ s^{-1} (Table 1) we find $\tau_{dw} \sim (1/k_{m,c-t}) + (1/k_w) \approx (40 \pm 8)$ ns. This estimate agrees reasonably very well with the one derived from the literature values of SO's distribution coefficient and diffusion constant (see Introduction). $\tau_l < \tau_{dw}$ indicates that most of the reactive oxygen species stay in the membrane long enough to react with the target, i.e. that τ_r is determined by τ_l. However, the values of τ_l and τ_{dw} are too close to each other to ensure a photodynamic efficiency of 100%. An increase in targeting efficiency can be realized by two different approaches: (i) by reducing the separation between PS and target so that other molecules susceptible to SO, like unsaturated lipids, cannot protect the proteinaceous target from encounters with SO and (ii) by increasing the quantum yield of PS molecules. Our model allows determining k_{Gen} in a membrane environment, thereby offering an important tool for PS optimization.

Data Availability

The datasets generated during and/or analyzed during the current study are available from the corresponding author on reasonable request.

References

1. O'Connor, A. E., Gallagher, W. M. & Byrne, A. T. Porphyrin and nonporphyrin photosensitizers in oncology: preclinical and clinical advances in photodynamic therapy. *Photochem Photobiol* **85**, 1053–1074, https://doi.org/10.1111/j.1751-1097.2009.00585.x (2009).
2. DeRosa, M. C. & Crutchley, R. J. Photosensitized singlet oxygen and its applications. *Coordin Chem Rev* **233**, 351–371, https://doi.org/10.1016/S0010-8545(02)00034-6 (2002).
3. *Photosensitizers in Medicine, Environment, and Security*. (Springer, 2012).
4. Baptista, M. S. *et al.* Type I and Type II Photosensitized Oxidation Reactions: Guidelines and Mechanistic Pathways. *Photochem. Photobiol.* **93**, 912–919, https://doi.org/10.1111/php.12716 (2017).
5. Rokitskaya, T. I., Block, M., Antonenko, Y. N., Kotova, E. A. & Pohl, P. Photosensitizer binding to lipid bilayers as a precondition for the photoinactivation of membrane channels. *Biophys J* **78**, 2572–2580 (2000).
6. Hackbarth, S., Bornhütter, T. & Röder, B. In *Singlet Oxygen: Applications in Biosciences and Nanosciences* Vol. 2, Ch. 26, 27–42 (The Royal Society of Chemistry, 2016).
7. Fischkoff, S. & Vanderkooi, J. M. Oxygen diffusion in biological and artificial membranes determined by the fluorochrome pyrene. *J. Gen. Physiol.* **65**, 663–676 (1975).
8. Hackbarth, S. & Roder, B. Singlet oxygen luminescence kinetics in a heterogeneous environment - identification of the photosensitizer localization in small unilamellar vesicles. *Photochem Photobiol Sci* **14**, 329–334, https://doi.org/10.1039/c4pp00229f (2015).

9. Battino, R., Evans, F. D. & Danforth, W. F. The solubilities of seven gases in olive oil with reference to theories of transport through the cell membrane. *J. Am. Oil Chem. Soc.* **45**, 830–833 (1968).
10. Cordeiro, R. M. Reactive oxygen species at phospholipid bilayers: Distribution, mobility and permeation. *Bba-Biomembranes* **1838**, 438–444, https://doi.org/10.1016/j.bbamem.2013.09.016 (2014).
11. Lavi, A., Weitman, H., Holmes, R. T., Smith, K. M. & Ehrenberg, B. The depth of porphyrin in a membrane and the membrane's physical properties affect the photosensitizing efficiency. *Biophys J* **82**, 2101–2110, https://doi.org/10.1016/S0006-3495(02)75557-4 (2002).
12. Mueller, P., Rudin, D. O., Tien, H. T. & Wescott, W. C. Metgods for the Formation of Single Bimolecular Lipid Membranes in Aqueous Solution. *J Phys Chem* **67**, 534–535, https://doi.org/10.1021/j100796a529 (1963).
13. Sokolov, V. S. & Pohl, P. Membrane transport of singlet oxygen monitored by dipole potential measurements. *Biophys. J.* **96**, 77–85, https://doi.org/10.1529/biophysj.108.135145 (2009).
14. Sokolov, V. S. & Kuz'min, V. G. Measurement of differences in the surface potentials of bilayer membranes according to the second harmonic of a capacitance current. *Biofizika* **25**, 170–172 (1980).
15. Ermakov, Y. A. & Sokolov, V. S. In *Planar Lipid Bilayers (BLMs) and their applications* (eds Tien, H. T. & Ottova-Leitmannova, A.) 109–141 (Elsevier, 2003).
16. Sokolov, V. S. & Mirsky, V. M. In *Ultrathin Electrochemical Chemo- and Biosensors*: *Technology and Performance* (ed. Mirsky, V. M.) 255–291 (Springer, 2004).
17. Sokolov, V. S. *et al*. Voltage-sensitive styryl dyes as singlet oxygen targets on the surface of bilayer lipid membrane. *J Photochem Photobiol B, Biology* **161**, 162–169, https://doi.org/10.1016/j.jphotobiol.2016.05.016 (2016).
18. Montal, M. & Mueller, P. Formation of Bimolecular Membranes from Lipid Monolayers and a Study of Their Electrical Properties. *Proc Natl Acad Sci USA* **69**, 3561–3566 (1972).
19. Horner, A., Antonenko, Y. N. & Pohl, P. Coupled diffusion of peripherally bound peptides along the outer and inner membrane leaflets. *Biophys. J.* **96**, 2689–2695, https://doi.org/10.1016/j.bpj.2008.12.3931 (2009).
20. Horner, A., Akimov, S. A. & Pohl, P. Long and short lipid molecules experience the same interleaflet drag in lipid bilayers. *Phys. Rev. Lett.* **110**, 268101, https://doi.org/10.1103/PhysRevLett.110.268101 (2013).
21. Magde, D., Elson, E. L. & Webb, W. W. Fluorescence correlation spectroscopy. II. *An experimental realization. Biopolymers* **13**, 29–61, https://doi.org/10.1002/bip.1974.360130103 (1974).
22. Cordeiro, R. M., Miotto, R. & Baptista, M. S. Photodynamic Efficiency of Cationic meso-Porphyrins at Lipid Bilayers: Insights from Molecular Dynamics Simulations. *J Phys Chem B* **116**, 14618–14627, https://doi.org/10.1021/jp308179h (2012).
23. Galambos, P. & Forster, F. K. In *Proceedings from the μTAS '98 Workshop*. (eds Harrison, D. J. & Van Den Berg, A.) 189–191 (Kluwer Academic Publishers: Dordrechht, Boston, London), (1998).
24. Rani, S. A., Pitts, B. & Stewart, P. S. Rapid diffusion of fluorescent tracers into Staphylococcus epidermidis biofilms visualized by time lapse microscopy. *Antimicrobial agents and chemotherapy* **49**, 728–732, https://doi.org/10.1128/aac.49.2.728-732.2005 (2005).
25. Bark, N., Földes-Papp, Z. & Rigler, R. The incipient stage in thrombin-induced fibrin polymerization detected by FCS at the single molecule level. *Biochem Biophys Res Commun* **260**, 35–41, https://doi.org/10.1006/bbrc.1999.0850 (1999).
26. Mozziconacci, J., Sandblad, L., Wachsmuth, M., Brunner, D. & Karsenti, E. Tubulin dimers oligomerize before their incorporation into microtubules. *Plos One* **3**, e3821, https://doi.org/10.1371/journal.pone.0003821 (2008).
27. Krasnovsky, A. A. *et al*. Quenching of singlet molecular oxygen by phthalocyanines and naphthalocyanines. *Photochem Photobiol* **55**, 691–696 (1992).
28. Subczynski, W. K., Hyde, J. S. & Kusumi, A. Oxygen permeability of phosphatidylcholine–cholesterol membranes. *Proc Natl Acad Sci USA* **86**, 4474–4478 (1989).
29. Widomska, J., Raguz, M. & Subczynski, W. K. Oxygen permeability of the lipid bilayer membrane made of calf lens lipids. *Biochim Biophys Acta Biomembr* **1768**, 2635–2645, https://doi.org/10.1016/j.bbamem.2007.06.018 (2007).
30. Rokitskaya, T. I., Kotova, E. A., Agapov, I. I., Moisenovich, M. M. & Antonenko, Y. N. Unsaturated lipids protect the integral membrane peptide gramicidin A from singlet oxygen. *FEBS Lett.* **588**, 1590–1595, https://doi.org/10.1016/j.febslet.2014.02.046 (2014).
31. Antonenko, Y. N. *et al*. Protective effects of mitochondria-targeted antioxidant SkQ in aqueous and lipid membrane environments. *J Membr Biol* **222**, 141–149, https://doi.org/10.1007/s00232-008-9108-6 (2008).
32. Egorov, S., Kurella, E. G., Boldyrev, A. A. & Krasnovsky, A. A. Jr. Quenching of singlet molecular oxygen by carnosine and related antioxidants. Monitoring 1270-nm phosphorescence in aqueous media. *Biochem Mol Biol Int* **41**, 687–694 (1997).
33. Krasnovsky, A. A. Jr. & Kagan, V. E. Photosensitization and quenching of singlet oxygen by pigments and lipids of photoreceptor cells of the retina. *FEBS Lett* **108**, 152–154 (1979).
34. Stozhkova, I. N., Cherny, V. V., Sokolov, V. S. & Ermakov Yu, A. Adsorption of haematoporphyrins on the planar bilayer membrane. *Membr Cell Biol* **11**, 381–399 (1997).
35. Engelmann, F. M. *et al*. Interaction of cationic meso-porphyrins with liposomes, mitochondria and erythrocytes. *J Bioenerg Biomembr* **39**, 175–185, https://doi.org/10.1007/s10863-007-9075-0 (2007).
36. Ehrenberg, B., Anderson, J. L. & Foote, C. S. Kinetics and yield of singlet oxygen photosensitized by hypericin in organic and biological media. *Photochem Photobiol* **68**, 135–140 (1998).

Acknowledgements

The work was supported in part by the Russian Science Foundation (grant #14-13-01373P) and by the Ministry of Education and Science of the Russian Federation in the framework of Increase of Competitiveness Program of "MISiS". The authors are grateful to Asya Vargaftik for the help with measurements and Quentina Beatty for editorial help.

Author Contributions

V.S.S. designed the experiments and wrote the manuscript, P.P. wrote the manuscript, O.V.B., S.A.A. and T.R.G. developed the theoretical model, A.N.K. and E.M. performed electrical measurements on planar bilayers, Y.G.G. provided compounds and advised on the chemistry of phtalocyanines, D.G.K. performed fluorescence measurements. All authors reviewed the manuscript.

Additional Information

Supplementary information accompanies this paper at https://doi.org/10.1038/s41598-018-31901-9.

Competing Interests: The authors declare no competing interests.

Publisher's note: Springer Nature remains neutral with regard to jurisdictional claims in published maps and institutional affiliations.